ELSEVIER

NeuroImage

www.elsevier.com/locate/ynimg
NeuroImage 31 (2006) 1525 – 1535

Unified framework for anisotropic interpolation and smoothing of diffusion tensor images

Arabinda Mishra,[a,*] Yonggang Lu,[a] Jingjing Meng,[b] Adam W. Anderson,[a,c] and Zhaohua Ding[a,b]

[a]*Institute of Imaging Science, Vanderbilt University, Nashville, 1161 21st Avenue South, MCN CCC-1118, TN 37232-2657, USA*
[b]*Department of Electrical Engineering and Computer Science, Vanderbilt University, Nashville, TN 37232-2657, USA*
[c]*Department of Biomedical Engineering, Vanderbilt University, Nashville, TN 37232-2657, USA*

Received 2 November 2005; revised 12 January 2006; accepted 16 February 2006
Available online 19 April 2006

To enhance the performance of diffusion tensor imaging (DTI)-based fiber tractography, this study proposes a unified framework for anisotropic interpolation and smoothing of DTI data. The critical component of this framework is an anisotropic sigmoid interpolation kernel which is adaptively modulated by the local image intensity gradient profile. The adaptive modulation of the sigmoid kernel permits image smoothing in homogeneous regions and meanwhile guarantees preservation of structural boundaries. The unified scheme thus allows piece-wise smooth, continuous and boundary preservation interpolation of DTI data, so that smooth fiber tracts can be tracked in a continuous manner and confined within the boundaries of the targeted structure. The new interpolation method is compared with conventional interpolation methods on the basis of fiber tracking from synthetic and in vivo DTI data, which demonstrates the effectiveness of this unified framework.

Keywords: Anisotropic interpolation; Smoothing; Diffusion tensor images

Introduction

Diffusion tensor imaging (DTI) is a magnetic resonance imaging modality capable of measuring the diffusive motion of water molecules in vivo (Basser et al., 1994; Le Bihan et al., 2001). An important utility of DTI is the tracking of neuronal fiber pathways (Jones et al., 1999; Conturo et al., 1999; Xue et al., 1999; Lazar et al., 2003; Ding et al., 2003), which draws upon the principle that the anisotropy of water diffusion reflects locally the directionality of fibrous tissues such as the brain white matter. Fiber tracking commonly starts from seed points predefined in a region of interest and proceeds along the dominant direction of the local diffusion tensor. Entire fiber pathways may be tracked in a streamline fashion by successively following the dominant tensor direction until certain termination criteria are met (Mori and van Zijl, 2002).

Fiber tracking with DTI, in essence, is the reconstruction of continuous curves from a direction field (Basser et al., 2000), which is typically noisy and discrete in nature. Noise is particularly harmful to fiber tracking because it deflects the fiber path directions and the impact accumulates during the tracking process (Anderson, 2001). To reduce noise, several smoothing algorithms for DTI data have been proposed, including Gaussian filtering (Westin et al., 2002), nonlinear smoothing (Parker et al., 2000; Chen and Hsu, 2005), anisotropic smoothing (Ding et al., 2005) and regularization approaches based on stochastic relaxation (Tench et al., 2002), Markovian random field (Poupon et al., 2000) or variational principles (Coulon et al., 2004; Wang et al., 2003). The discrete nature of DTI data, on the other hand, necessitates the interpolation of the direction field for continuous curves to be obtained. To date, a few well-established methods from the repository of classical image interpolation techniques have been empirically chosen for this purpose, such as linear (Tournier et al., 2002), low order polynomial (Xu et al., 2002; Gossl et al., 2002), cubic b-spline (Pajevic et al., 2002) and nearest neighbor interpolations (Mori et al., 1999). Smoothed and interpolated direction field allows fiber pathways to be tracked more reliably and in a continuous manner.

While the primary goal of noise reduction and interpolation is to generate a piece-wise smooth and continuous direction field, preservation of structural boundaries in DTI data is also a desirable property that should be considered. Structural boundaries define the spatial range of individual structures, and hence offer a natural means of confining fiber tracking, or any other region growing processes for image segmentation, within specific structures. Inadequate boundary preservation often leads to the spreading of fiber pathways into neighboring structures, which is manifested as erroneous connections between distinct fiber bundles encountered in many fiber-tracking algorithms. Moreover, because DTI data inherently contain a large number of structural boundaries, due to the superior capability of DTI to provide fine contrast between different fiber bundles, the need for boundary preservation is particularly imperative for DTI data processing.

* Corresponding author. Fax: +1 615 322 0734.
E-mail address: arabinda.mishra@vanderbilt.edu (A. Mishra).
Available online on ScienceDirect (www.sciencedirect.com).

1053-8119/$ - see front matter © 2006 Elsevier Inc. All rights reserved.
doi:10.1016/j.neuroimage.2006.02.031

Although preservation of structural boundaries has been addressed by some of the smoothing algorithms mentioned above (Parker et al., 2000; Chen and Hsu, 2005; Ding et al., 2005; Coulon et al., 2004; Wang et al., 2003), few existing DTI interpolation methods possess this capability. Indeed, except the nearest neighbor interpolation, which necessarily incurs discontinuity artifacts, all other interpolation methods that have been used for DTI data thus far suffer from boundary blurring. The present study is therefore motivated by the need for a smooth, continuous and boundary preserving interpolation of DTI data so that smooth fiber pathways can be reconstructed continuously and confined within the boundaries of targeted structures. To this end, we have developed an anisotropic interpolation technique that preserves structural boundaries and meanwhile ensures continuity of interpolated direction field. Similar to the provocative conception of anisotropic smoothing for enhancing flow-like structures (Weickert, 1999), the anisotropic interpolation kernel we designed is adaptable to the local image intensity gradient profile, which is a function of the strength and orientation of the structural boundaries. Furthermore, we integrated the anisotropic interpolation with image smoothing to establish a single unified framework that has the functionality of noise reduction as well. We expect improved fiber-tracking accuracy to be gained with this integrated interpolation and smoothing scheme.

The remainder of this paper is organized as follows. Section 2 presents the proposed framework for integrated interpolation and smoothing in detail. Section 3 describes fiber-tracking experiments using our integrated scheme on both synthetic and in vivo human DTI data. Section 4 presents the results of fiber tracking and compares the effectiveness of our interpolation approach with conventional interpolation methods. Section 5 discusses relevant technical issues, followed by concluding remarks.

Methods

Interpolation is a classical image processing problem for which a variety of methods exist (Lehmann et al., 1999). The methods differ in frequency response, extent of support, computational complexity and degree of continuity of the interpolated image. The critical component of any interpolation technique is the interpolation kernel, which distinguishes different interpolation techniques and determines their performance in the spatial and frequency domain. Conventional interpolation kernels are isotropic and space-invariant (kernel profiles are invariable irrespective of orientation and position) and hence have the drawback of disregarding local image features, such as structural boundaries. As mentioned before, DTI data have abundant structural boundaries that need to be preserved during interpolation to facilitate fiber tracking. This evidently requires the interpolation kernel to be space-variant so that structural boundaries can be handled differently from homogeneous regions.

Space-variant anisotropic image interpolation

In designing the kernel for boundary preserving interpolation of DTI data, we bear the following considerations in mind. (1) Space-variant: the interpolation kernel is a function of local image features, i.e., it takes on different profiles for structural boundaries and homogeneous regions. (2) Anisotropy: it retains high-frequency components (sharp intensity contrast) across structural boundaries but low-frequency components (smooth intensity transition) along structural boundaries. (3) Smoothing: it suppresses noise without compromising the sharpness of structural boundaries. Given the above, the interpolation kernel is designed to be an adaptive sigmoid function with sharpness of the kernel anisotropically modulated by the local image intensity gradient. Since the local intensity gradient is directly related to the strength and orientation of structural boundaries, this adaptive and anisotropic interpolation kernel can be tuned to satisfy the first two considerations. As will also become clear soon, the desirable functionality of boundary-preserving noise suppression can be served with this interpolation kernel as well.

Eq. (1) below is the sigmoid kernel function that governs the interpolation process for 1D case:

$$f(x) = (1 + \exp(a \times (x - \eta)))^{-1} \quad (1)$$

where the range of x is [0, 1). The profile of the function $f(x)$ depends on the value of a and η, with a regulating the sharpness of the function and η controlling the position of maximum change in magnitude. To illustrate, Fig. 1 shows the profiles of $f(x)$ for η = 0.5 with different values of a (Fig. 1(a)) and their corresponding frequency responses (Fig. 1(b)). It can be seen that a larger a gives a sharper f whose frequency response has larger high-frequency components. Evidently interpolation with a sharper f retains more

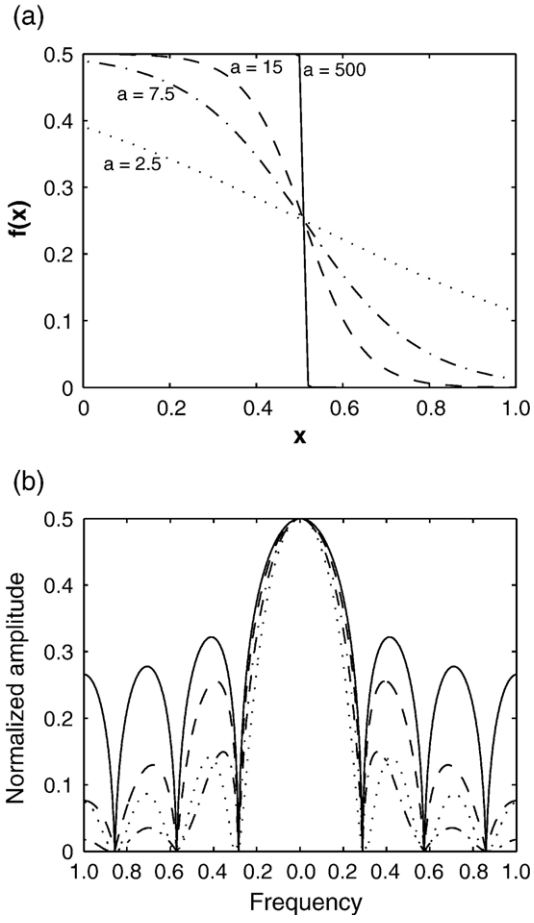

Fig. 1. (a) Profiles of 1D sigmoid function with different values of shape control parameter a, and (b) their corresponding frequency responses. Line styles denote different values of a.

high-frequency components (than with a flatter f). In particular, when a approaches infinity, f becomes a step function which corresponds to a nearest neighbor interpolation. Conversely, when a is 0, f becomes a constant with a value of 0.5, which corresponds to a linear interpolation with averaged neighborhood value (smoothing). Between the two extremes, the kernel function may have various degrees of sharpness and smoothing depending on the choice of a.

For space-variant, anisotropic interpolation of 2D or 3D scalar images, we may adapt the sharpness of the sigmoid function to the local image intensity gradient. A simple formulation relates the parameter a to the magnitude of the intensity gradient along each spatial direction, i.e.,

$$a_i = g(|\nabla I_i|) \quad i \in \{1,2\} \text{ or } \{1,2,3\} \tag{2}$$

where subscript i denotes the ith spatial direction, $|\nabla I|$ is the magnitude of the gradient, and $g(.)$ is a linear function.

At structural boundaries, the sigmoid function is sharper across the boundary than along it due to a greater gradient across the boundary. Interpolation with this kernel thus preserves sharp intensity contrast across the structural boundaries and meanwhile permits certain smoothing along the boundaries. In homogeneous regions, the sigmoid function tends to be flat and isotropic which allows interpolation with similar smoothing along all spatial directions. This space-variant and anisotropic behavior of the sigmoid interpolation is illustrated in Fig. 2, which schematically shows the profiles of two 2D kernels (outer product of 1D kernels) in a homogeneous region and at a structure boundary respectively.

In our design, the linear function $g(.)$ that relates parameter a and the image intensity gradient ∇I is defined as follows:

$$a_i = g(|\nabla I_i|) = a_{\min} + (a_{\max} - a_{\min}) \times \left| \frac{\nabla I_i}{\nabla I_{i\max}} \right| \tag{3}$$

where $|\nabla I_{\max}|$ is the maximum intensity gradient of the image; $a_{\max}$ and $a_{\min}$ delimit the linear mapping between a and $|\nabla I|$, so that a will fall into a proper range. Well-defined values of $a_{\max}$ and $a_{\min}$ allow adjustment of the sharpness across structural boundaries and smoothness along structural boundaries and in homogeneous regions to a desired level. Throughout this paper, $a_{\min}$ is chosen to be zero.

Interpolation tests with a 2D scalar image

The anisotropic interpolation technique designed has been tested with a 2D scalar image (a tile image that contains a large number of structural boundaries), as shown in Fig. 3. The objective is to study the performance of this algorithm at structural boundaries and in homogeneous regions and to compare with other conventional interpolation methods. First, zero mean Gaussian noise is added to the original image to generate a noisy image (Fig. 3(a)) with a signal-to-noise ratio (SNR, defined as mean signal intensity divided by standard deviation of noise) of 16.67. This noisy image is then enlarged eight times using linear, nearest neighbor, cubic polynomial, spline and anisotropic interpolation (with $a_{\max}$ = 30) methods respectively.

Figs. 3(b–f) are the set of interpolated images of the boxed area in (a). It can be seen that the anisotropic interpolation is superior to all the other methods with respect to boundary preservation and noise reduction. Linear interpolation (b) produces a smoothly interpolated image with certain effect of noise reduction, but blurs structural boundaries due to the use of a space-invariant and isotropic linear kernel. Nearest neighbor interpolation (c), on the other hand, does not have any noise reduction capability and meanwhile creates sharp discontinuity at the structural boundaries (manifested as jagged edges). Both cubic polynomial (d) and spline (e) interpolations give results similar to that of linear interpolation, but with less smoothing effect. In contrast, anisotropic interpolation (f) yields an image with sharp and continuous structural boundaries (manifested as clear and smooth edges) and with significantly reduced noise in homogeneous regions and along structural boundaries. This is

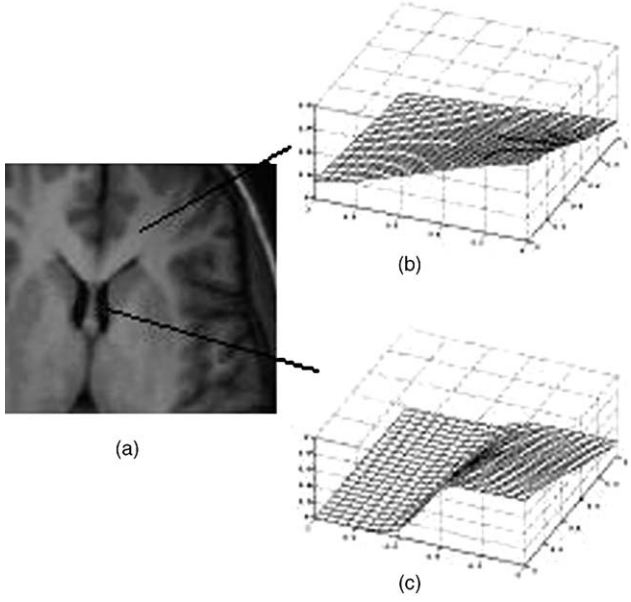

Fig. 2. Examples of 2D sigmoid interpolation kernel. (a) A gray-level image. (b) An isotropic interpolation kernel in a homogeneous region. (c) An anisotropic interpolation kernel at a structure boundary.

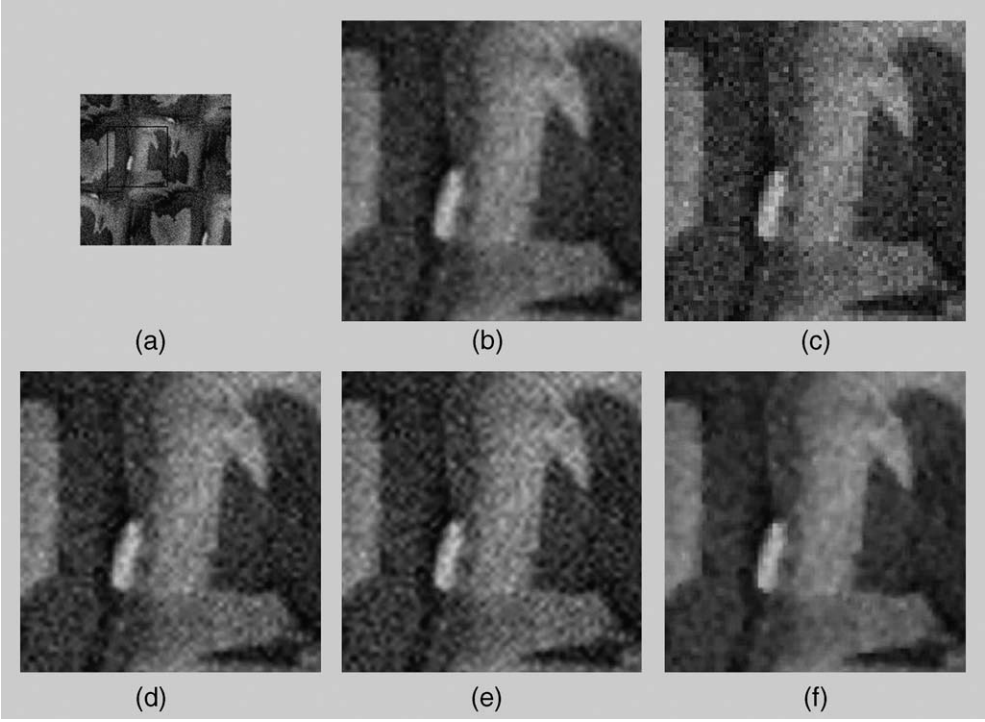

Fig. 3. Interpolation of a 2D scalar image in panel a using linear (b), nearest neighbor (c), cubic polynomial (d), spline (e) and anisotropic interpolation (f). Panels b–f correspond to the boxed area in panel a.

attributable to the use of an anisotropic sigmoid interpolation kernel that is adaptively modulated by the local image gradient profile.

Anisotropic interpolation of diffusion tensor images

In DTI, the diffusion of water molecules within a voxel is characterized by a second order, symmetric 3 × 3 tensor matrix. Since a symmetric tensor matrix has six degrees of freedom with six independent components (Westin et al., 2002), to interpolate the DTI data, we may simply apply the anisotropic interpolation as described above to each of the six components separately or to them jointly with a single interpolation kernel. The latter alternative is chosen in this study as it yields better data consistency (tensor orientational coherence and positive definiteness). Specifically, we fix η to be 0.5 but modulate a linearly with the mean intensity gradient of the six independent components along each spatial direction according to equations below and Eq. (3):

$$|\nabla I_i| = \frac{1}{6} \times (|\nabla I_{ic_{11}}| + |\nabla I_{ic_{22}}| + |\nabla I_{ic_{33}}| + |\nabla I_{ic_{12}}| + |\nabla I_{ic_{13}}| + |\nabla I_{ic_{23}}|) \quad (4)$$

$$c_{jk}(t_i + \Delta t_i)\Big|_{\substack{j=1\cdots3 \\ k=1\cdots3}} = c_{jk}(t_i) \times (1 + \exp(a_i \times (\Delta t_i - \eta)))^{-1} + c_{jk}(t_i + 1) \times (1 - (1 + \exp(a_i \times (\Delta t_i - \eta)))^{-1}) \quad (5)$$

$$i \in \{1, 2, 3\}$$

where $c_{11},\ldots, c_{23}$ denote the independent components of the tensor matrix. Eq. 5 explains the interpolation of the tensor elements where t_i is an integer that denotes the discrete coordinate of a voxel and $\Delta t_i \in [0,1]$ is a real number that specifies the spatial location for interpolation.

Fiber-tracking experiments

To assess the performance of the anisotropic interpolation technique, effects of the interpolation on fiber tracking were examined and compared with other conventional methods using both synthetic and in vivo DTI data. Fiber tracking was implemented using the principal diffusion direction method, i.e., the so-called "streamline" tracking approach (Basser et al., 2000). Although more sophisticated fiber-tracking methods could be used (Lu et al., in press), we deliberately chose this simple, intuitive fiber-tracking approach because it is widely accepted, and more importantly, it allows us to evaluate and interpret the impact of various interpolation techniques without other confounds. For all the synthetic and in vivo data, streamline fiber tracking was performed with a step size of 0.2 voxel and termination criteria of FA < 0.15 and turning angle >45°. Four different values of $a_{\max}$, i.e., 5, 10, 15 and 20, were used respectively for the anisotropic interpolation. Tracking results obtained using our anisotropic interpolation technique were compared with those generated by four conventional interpolation methods that include linear, nearest neighbor, cubic polynomial and spline interpolations.

Fiber tracking with synthetic data

Two sets of synthetic data were designed to test the efficiency, accuracy and precision of fiber tracking. The first dataset consisted of parallel 3D spirals and the second contained parallel straight lines. These two basic configurations were chosen because of their simple algebraic constructions and analytically derivable solutions for the true "fiber" path. The 3D spirals had a rectangular cross-section of 3 × 9 voxels and spanned two full cycles (from 0 to 4π), as shown in Fig. 4. Both synthetic "fiber" sets were noise free and

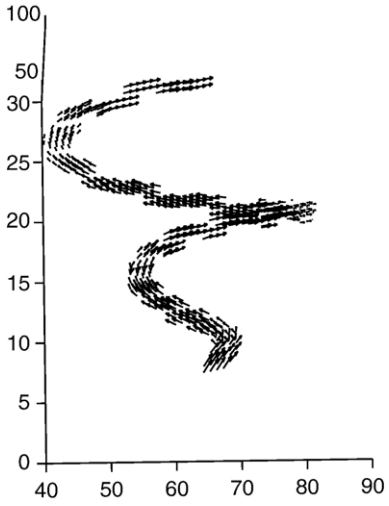

Fig. 4. A 3D view of the synthetic spirals. The spirals have a rectangular cross-section, span two full cycles and are embedded in isotropic media (not shown). The line segments are the directions of the principal eigenvector.

embedded in isotropic media that had zero fractional anisotropy (FA = 0).

To closely mimic the in vivo conditions, the synthetic tensors were constructed to have a trace of 2.1×10^{-5} cm^2/s, comparable to that in normal brain parenchyma. Tensors for the "fiber" tracts were cylindrically symmetric with an FA of 0.9 and aligned with the local tangential direction of the tract. The whole volume of each synthetic dataset (including the isotropic region) had a dimension of $128 \times 128 \times 30$ voxels with a spatial resolution of $2 \times 2 \times 2$ mm^3. Diffusion-weighted images were calculated for both geometries, with diffusion weighting simulated along six non-collinear directions with a b-value of 1000 s/mm^2.

Test of tracking efficiency

Tracking efficiency was tested on the synthetic dataset that contains the 3D spirals. Fiber tracking was initiated from the base of the spirals, specifically from the center of each voxel in the anisotropic region at the starting cross-section. Fibers were terminated when any of the termination criteria were met.

Performance comparisons between the anisotropic interpolation and conventional methods were made on the basis of the mean length of reconstructed "fibers" and similarity coefficient. The similarity coefficient was defined to be the mean shape similarity between each "fiber" and the true tract, with the shape similarity computed according to the equation below for an arbitrary pair of fibers:

$$S_{ij} = R_{\mathrm{cs}} \cdot \exp(-\sigma/C) \tag{6}$$

where i, j denote two fibers, R_{cs} is the corresponding segment ratio between i and j (motivated by the work of Ding et al., 2003), σ is the standard deviation of the Euclidian distance between the corresponding segments, and C is a scaling constant. Like the definition in Ding et al., the corresponding segment ratio R_{cs} is the ratio of the overlapping portion of two fibers to the total length they span; the Euclidian distance between the corresponding segments is calculated point-wise along the "fiber" on the basis of the coordinates of corresponding points. But unlike the previous work, the standard deviation of the Euclidian distance instead of its mean is used in Eq. (6). The reason is that the original work of Ding et al. was focused on bundling of fibers which relies on the shape similarity as well as spatial proximity between a pair of fibers, whereas the present work is only concerned with how a "fiber" takes the shape of its true tract. Therefore, the standard deviation of the Euclidian distance between them better serves the purpose.

The shape similarity defined as above has a range between 0 and 1, with two fibers of comparable length and similar shape having a higher similarity value. As in this study, the longest fiber is used as the true tract for similarity calculation, fibers consistent with this tract in shape and length can have a similarity coefficient close to one.

To characterize the overall efficiency of fiber tracking, a measure, *tracking efficiency* was defined which is the product of mean fiber length (normalized by the true fiber length) and similarity coefficient. Because we have selected a narrow "fiber" strip in the synthetic data intentionally, a small deviation from the true path may result in premature termination of the "fiber". This is due to the anisotropy of the media surrounding the spirals, which however can provide a rigorous test of tracking efficiency.

Test of tracking accuracy and precision

To evaluate the accuracy and precision of fiber tracking using our interpolation approach and other conventional methods, Monte Carlo simulations were performed on the second dataset which contains parallel straight "fiber" tracts. In these simulations, zero mean Gaussian noise was added to the synthetic data to generate four noisy datasets at SNR of 10, 20, 30 and 40 respectively (independently to each tensor component with the same variance). Like the first dataset, a rectangular seed region of 3×9 equally spaced grid points was defined within the starting cross-section of the synthetic "fibers". At each noise level, streamline fiber tracking from the above seed region was performed 100 times, each time with a different random realization of zero mean Gaussian noise. A total of 100 steps were tracked, and the mean Euclidian distance and standard deviation with respect to the true "fiber" tract were assessed at each step for all noise levels and interpolation methods. These two parameters measure the accuracy and precision or consistency of fiber tracking using different interpolation methods.

Fiber tracking with in vivo human DTI data

The in vivo DTI data presented for analysis were acquired from a healthy human volunteer on a 3T GE Signa MR scanner using diffusion weighted single shot, echo plannar pulsed gradient spin echo imaging sequence. Diffusion weighting was performed along six non-collinear directions with a b-value of 1000 s/mm^2 and timing parameters of TR = 9 s and TE = 88.5 ms. Thirty contiguous, 4-mm-thick slices with a matrix size of 128×128 and a field of view of 240×240 mm^2 were scanned and reconstructed into a 256×256 matrix, resulting in an in-plane resolution of 0.937×0.9375 mm^2. A total of 37 repeated acquisitions were performed, but a small portion of these with motion and other artifacts were discarded. The remaining high quality data were used for tensor calculations (Basser et al., 1994), from which FA maps were computed. Prior to the study, informed consent was

obtained from the subject in accordance with the protocols approved by the local ethics committee.

Due to the lack of a "gold standard" which makes it impossible to quantify the accuracy of fiber tracking, evaluation of the interpolation methods was based on qualitative assessment of the fiber bundles reconstructed. For this purpose, two major fiber bundles, namely the projection pathways (the corticospinal tracts) and the corpus callosum, were reconstructed which provide the basis for methods comparison. These fiber bundles were chosen because of their well-known anatomy which facilitates judgment of the quality of reconstructed fiber pathways and identification of possible erroneous connections. Streamline fiber tracking with different interpolation methods was launched from seed points defined in the above fiber bundles and terminated when one of the termination criteria was met.

Results

Tracking efficiency

Fig. 5 graphically shows the "fibers" tracked from the synthetic 3D spirals using conventional interpolation methods (a–d) and our anisotropic interpolation approach with different values of a_{max} (e–h). It can be seen that results from the anisotropic interpolation are more favorable because in general it yields a greater number of "fibers", and the pathways of these "fibers" are more consistent than those obtained with conventional interpolation methods. These results are quantitatively compared in Table 1, which summarizes the mean length (normalized by the ideal length), similarity coefficient, and tracking efficiency for four conventional interpolations (linear, nearest neighbor, cubic poly-

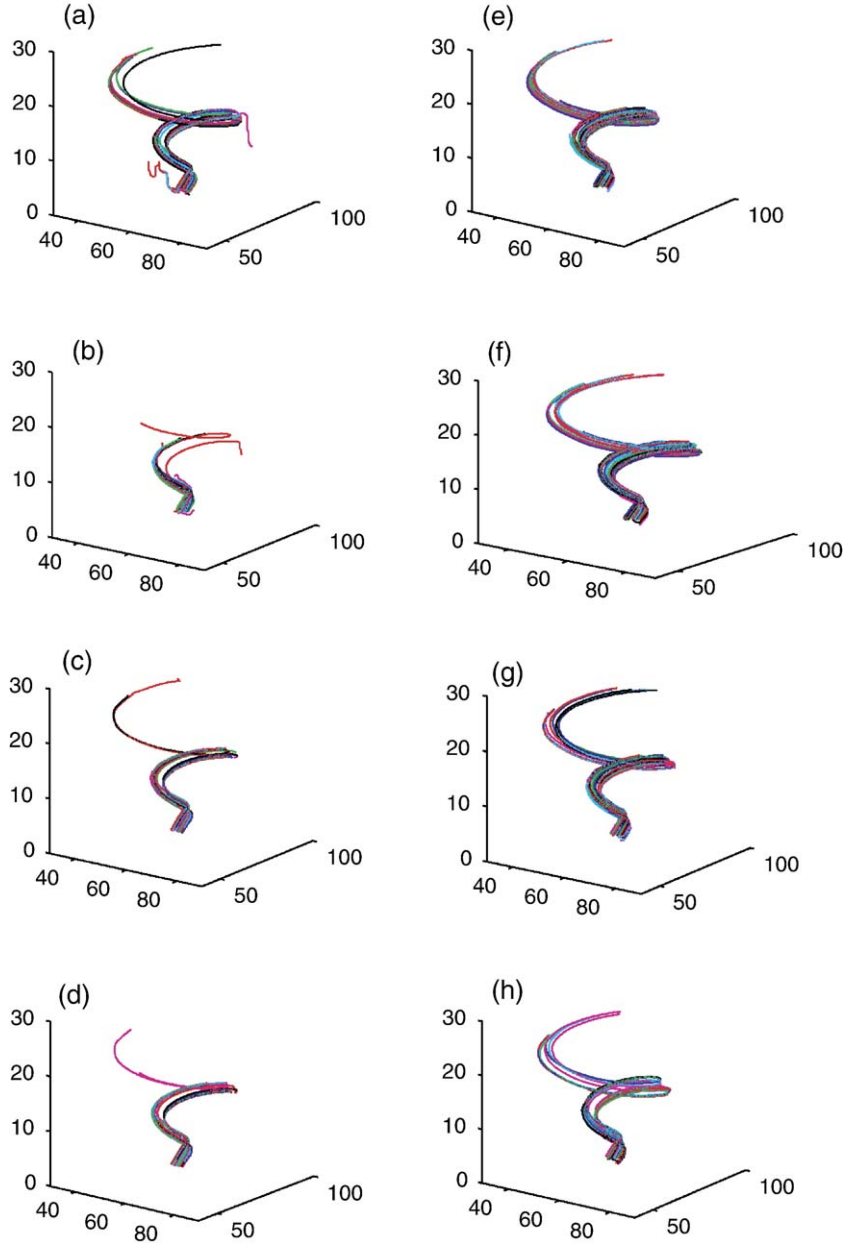

Fig. 5. "Fiber" tracts reconstructed from the synthetic spirals. Panels a–d are from linear, nearest neighbor, cubic polynomial and spline interpolations respectively. Panels e–h are from the anisotropic interpolation with a_{max} = 5, 10, 15 and 20 respectively.

Table 1
Comparisons of similarity coefficient, mean length and tracking efficiency between four conventional interpolation methods and the anisotropic interpolation with noiseless synthetic spirals

Interpolation method	Similarity coefficient	Mean length	Tracking efficiency
Linear	0.2924	0.8538	0.2496
Nearest neighbor	0.7548	0.2917	0.2201
Cubic polynomial	0.4092	0.7823	0.3201
Spline	0.4822	1.0000	0.4822
Anisotropic			
a_{max} = 5	0.4127	0.8181	0.3376
a_{max} = 10	0.7023	0.9105	**0.6394**
a_{max} = 15	0.7492	0.8341	**0.6249**
a_{max} = 20	0.4362	0.6988	0.3048

Bold numbers denote the largest values of tracking efficiency.

nomial and spline) and the anisotropic interpolation with a_{max} = 5, 10, 15 and 20 respectively. Linear, cubic polynomial and spline interpolations tend to give reasonably long "fibers", but the similarity coefficient is quite low; nearest neighbor interpolation gives more consistent "fibers", but their mean length is much smaller than that from other methods. By comparison, "fibers" from the anisotropic interpolation with a_{max} = 10 and 15 are both reasonably long and consistent; this is reflected as higher values of overall tracking efficiency (last column) than the other interpolation methods.

Tracking accuracy and precision

Tests of the accuracy and precision of fiber tracking using Monte Carlo simulations found that, at all noise levels and tracking steps, the anisotropic interpolation with $a_{max} > 5$ has smaller mean Euclidian distance and standard deviation than the conventional interpolation methods. As an example, Fig. 6 shows variations of the mean Euclidian distance (a) and standard deviation (b) with the number of tracking steps for a typical noise level (SNR = 20). Quantitative comparisons of these measures at 100 tracking steps and four different noise levels are given in Table 2, which shows overall there is ~20% improvement in the mean Euclidian distance and ~40% improvement in the standard deviation with the anisotropic interpolation particularly when $a_{max} > 5$. To better appreciate the improvements, the data in Table 2 are plotted as bar graph in Fig. 7 with both the mean Euclidian distance and standard deviation normalized to 0.5. These clearly demonstrate that the anisotropic interpolation gives better tracking accuracy and precision than the conventional methods.

Fiber tracking with in vivo data

Fig. 8 shows the axial view of the anatomic structure of a fiber bundle in the corpus callosum using conventional interpolation methods (a–d) and the anisotropic interpolation approach (e–h) for fiber tracking. Linear interpolation (a) gives fibers similar to anisotropic interpolation with a_{max} = 5 but generates fewer fibers than anisotropic interpolation with a_{max} = 15–20 (pointed by green arrow in (a)). Nearest interpolation (b) gives fewest fibers than any other methods due to the inherent noise sensitivity of the method (see green arrow in (b)). Fibers tracked with cubic polynomial (c) and spline (d) interpolations have possibly wrong connections (pointed by green arrows). These questionable connections, however, are not present in the fibers tracked with the anisotropic interpolation. In our interpolation approach, although major patterns of the fiber tracts are grossly similar, different values of a_{max} bring appreciable differences to the fiber structure, with the outcomes with a_{max} = 10 (f) and 15 (g) being more plausible. Another illustration in Fig. 9 shows similar variations of fiber structures. Fibers from linear interpolation (a) are similar to those from anisotropic interpolation with a_{max} = 5 (e). Nearest interpolation (b) again generates fewest fibers than any other methods (see cyan arrow in (b)). Cubic polynomial (c) and spline (d) interpolations and to some extent anisotropic interpolation with a_{max} = 20 (h) have generated dense fibers at the branching points (pointed by cyan arrows), which is likely due to connection loops that are erroneously formed. These loops, however, do not exist in anisotropic interpolation with a_{max} = 5–15. The blue arrows in Figs. 9(d, e, h) indicate a prominent erroneous pathway at the base of the fiber bundle. This fiber is absent in anisotropic interpolation for a_{max} = 10 and 15.

Discussions and conclusion

Image smoothing and interpolation play critical roles in DTI-based fiber tractography. Smoothing reduces the detrimental effect

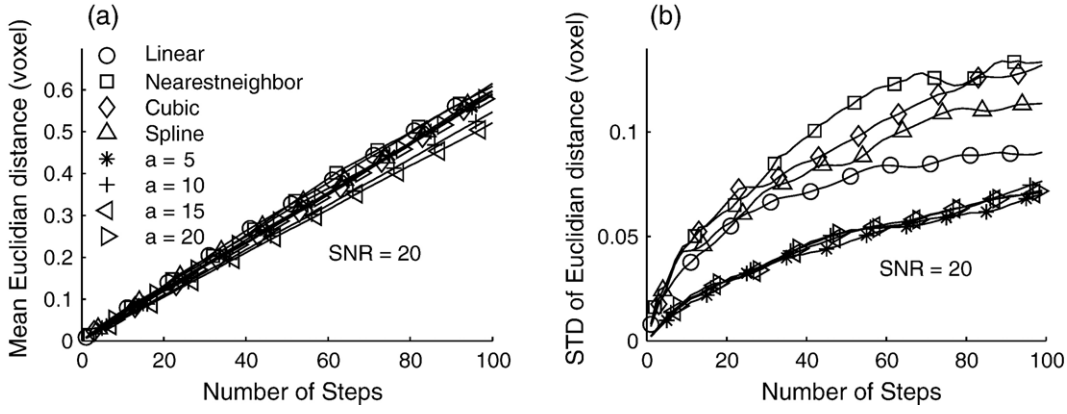

Fig. 6. Variations of mean Euclidian distance (a) and standard deviation (b) versus the number of tracking steps with SNR = 20. Different symbols denote different interpolation methods.

Table 2
Comparisons of the mean Euclidian distance and standard deviation at 100 tracking steps between four conventional interpolation methods and the anisotropic interpolation

Interpolation methods	Mean Euclidian distance (voxels)				Standard deviation (voxels)			
	SNR = 10	SNR = 20	SNR = 30	SNR = 40	SNR = 10	SNR = 20	SNR = 30	SNR = 40
Linear	1.3156	0.6155	0.4193	0.2377	0.2070	0.0966	0.0721	0.0558
Nearest neighbor	1.3089	0.6093	0.3999	0.2515	0.3035	0.1196	0.0929	0.0726
Cubic polynomial	1.3448	0.5970	0.4118	0.2413	0.2653	0.1149	0.0884	0.0636
Spline	1.2768	0.5983	0.4090	0.2464	0.2399	0.1100	0.0815	0.0600
Anisotropic								
$a_{max} = 5$	1.2866	0.6104	0.3927	0.2504	0.1432	0.0701	0.0454	0.0327
$a_{max} = 10$	1.1337	0.5349	0.3385	0.2053	0.1370	0.0684	0.0423	0.0342
$a_{max} = 15$	1.0546	0.4976	0.3149	0.1910	0.1554	0.0694	0.0442	0.0356
$a_{max} = 20$	1.1111	0.5242	0.3317	0.2012	0.1403	0.0666	0.0441	0.0316

Measures are given for four noise levels.

of noise on fiber tracking, and interpolation allows continuous fiber tracts to be reconstructed. These two needs are met in this study by a unified framework for interpolation and smoothing. The core part of this framework is a sigmoid interpolation function that is anisotropically modulated by the local profile of image intensity gradient. The integrated, adaptive scheme not only avoids the awkward separation of two mutually related processes for fiber tracking but also preserves structural boundaries which are important for confining fiber tracts within the specific structure of interest. Experiments with synthetic DTI data demonstrate that performance of fiber tracking in terms of tracking efficiency, accuracy and precision can be enhanced, and fiber tracking with in vivo data shows that more plausible fiber tracts can be obtained using this unified framework.

As mentioned before, there are a plethora of classical methods for image interpolation. Among these, two basic interpolation methods, i.e., linear and nearest neighbor interpolation, arguably represent two extremes of interpolation. Linear interpolation is a "smoothing operator" that suppresses high spatial frequencies (due to noise or presence of structural boundary) to some extent and therefore tends to allow fiber tracking to naturally cross the structural boundary. On the other hand nearest neighbor interpolation acts as a "high pass operator" that preserves the boundary information, but the high-frequency components particularly from image noise may lead to premature termination of the fibers. Polynomial and spline interpolation seems to lie between the two extremes, as is evident from their profiles in the spatial domain (not shown), but they tend to behave more like linear interpolation in

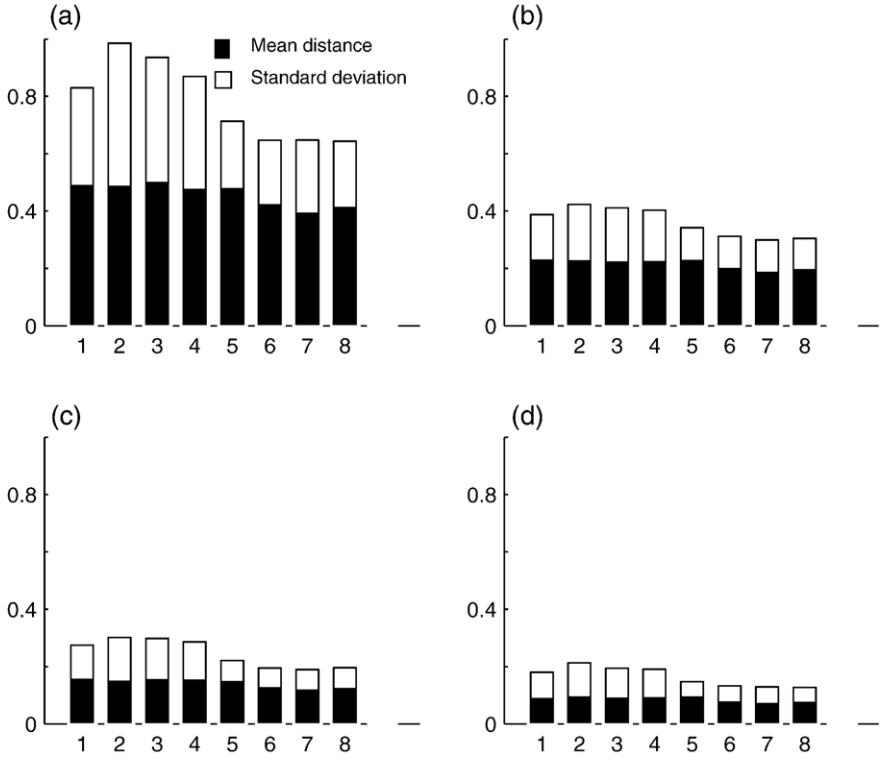

Fig. 7. Bar graph schematically showing the data in Table 2. The values of both statistical measures are normalized against 0.5 and stacked for each interpolation method with different levels of SNR (a. 10, b. 20, c. 30, d. 40). Numbers on x-axis represent different methods 1. linear, 2. nearest neighbor, 3. cubic polynomial, 4. spline, 5–8. anisotropic interpolation with $a_{max} = 5$, 10, 15 and 20 respectively.

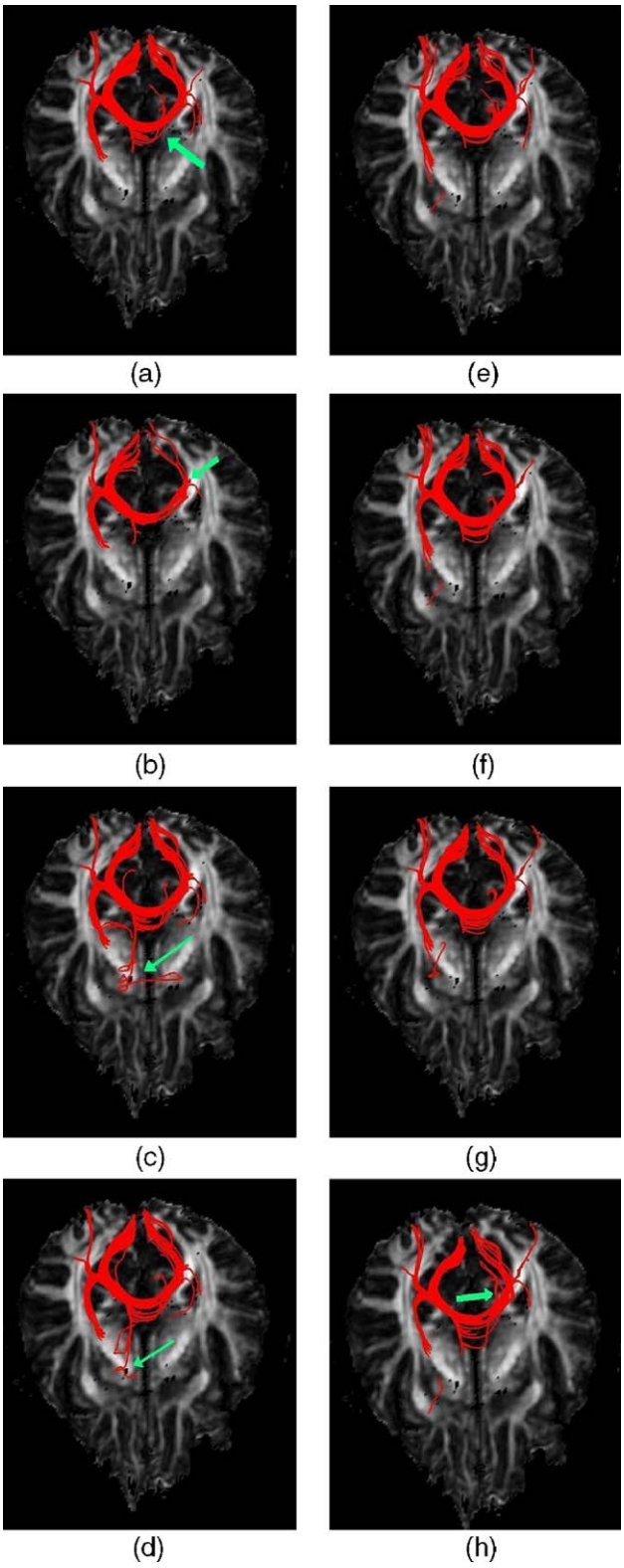

Fig. 8. Axial view of reconstructed fibers seeded in the corpus callosum. Panels a–d are from linear, nearest neighbor, cubic polynomial and spline interpolations respectively, and panels e–h are from the anisotropic interpolation with a_{max} = 5, 10, 15 and 20 respectively. Arrows in panels a, b point to missed fibers, and arrows in panels c, d, h point to possibly wrong connections.

fiber tracking for the termination criteria used in this study. The impact of these conventional interpolation methods on fiber tracking can be seen graphically in Figs. 5–9 and quantitatively in Tables 1 and 2. The design of our interpolation kernel addresses two conflicting needs, i.e., suppression of image noise and preservation of structural boundaries, with a sigmoid function that is adaptive to the local image intensity gradient. It offers an augmented capability for reducing random noise typically present in DTI data. Such an interpolation kernel behaves like an "adaptive operator", which suppresses random noise in homogenous regions where image intensity gradient is low and preserves structural boundaries where intensity gradient is high. This adaptive operation translates to improved performance in fiber tracking, which is seen from the experiments on synthetic as well as in vivo DTI data throughout this study.

The performance gain in fiber tracking with our interpolation scheme comes from the shape control parameter a of the sigmoid function, which is linearly modulated with the strength of the local image intensity gradient in this study. It should be noted that choosing this simple linear modulation is purely empirical. While the simplicity offers convenience in implementation and standardization of the interpolation procedure, more sophisticated parameter modulation schemes may also be designed without undue complications. For example, one may relate the parameter a with the noise level such that image noise can be maximally suppressed in homogeneous regions and high-frequency information at structural boundaries maximally preserved, which may further improve the performance of fiber tracking. Nevertheless, we reserve these and other refinements of the modulation model for future studies.

We have studied a range of values for the maximum kernel sharpness parameter a_{max}, specifically from a_{max} = 5 to 20, for the anisotropic interpolation kernel. Our fiber-tracking experiments from synthetic and in vivo DTI data suggest that a_{max} = 10–15 tend to give the best overall tracking performance. However, this empirical observation is only based on experiments with our specific geometric and imaging settings; no rigorous theoretical justification of this choice has been performed. We therefore caution that, in application of the anisotropic interpolation to a specific fiber-tracking experiment, fine tuning of this parameter is warranted to yield the best tracking performance.

It is worth mentioning that the sigmoid interpolation kernel used in this study has a very compact support. Only eight neighboring voxels are involved in the case of 3D data interpolation, similar to linear and nearest neighbor interpolation but smaller than cubic polynomial and spline interpolation. Computational efficiency of the interpolation is slightly less than that of the conventional interpolation methods as it involves calculations of image intensity gradient, but the amount of additional computation needed is quite small. It should be noted that, as the image gradients are calculated along coordinate axes, the procedure inherently favors boundaries aligned along these directions. Image gradients in fact can be computed in any directions so that structural boundaries along an arbitrary direction can be preserved. However, this may come at the cost of computational efficiency. It should be also pointed out that, although the unified framework has a built-in functionality of noise reduction, its smoothing capability is nevertheless limited. Therefore, in the case of heavy image noise in DTI data, presmoothing such as performed in Ding et al. (2005) is still necessary.

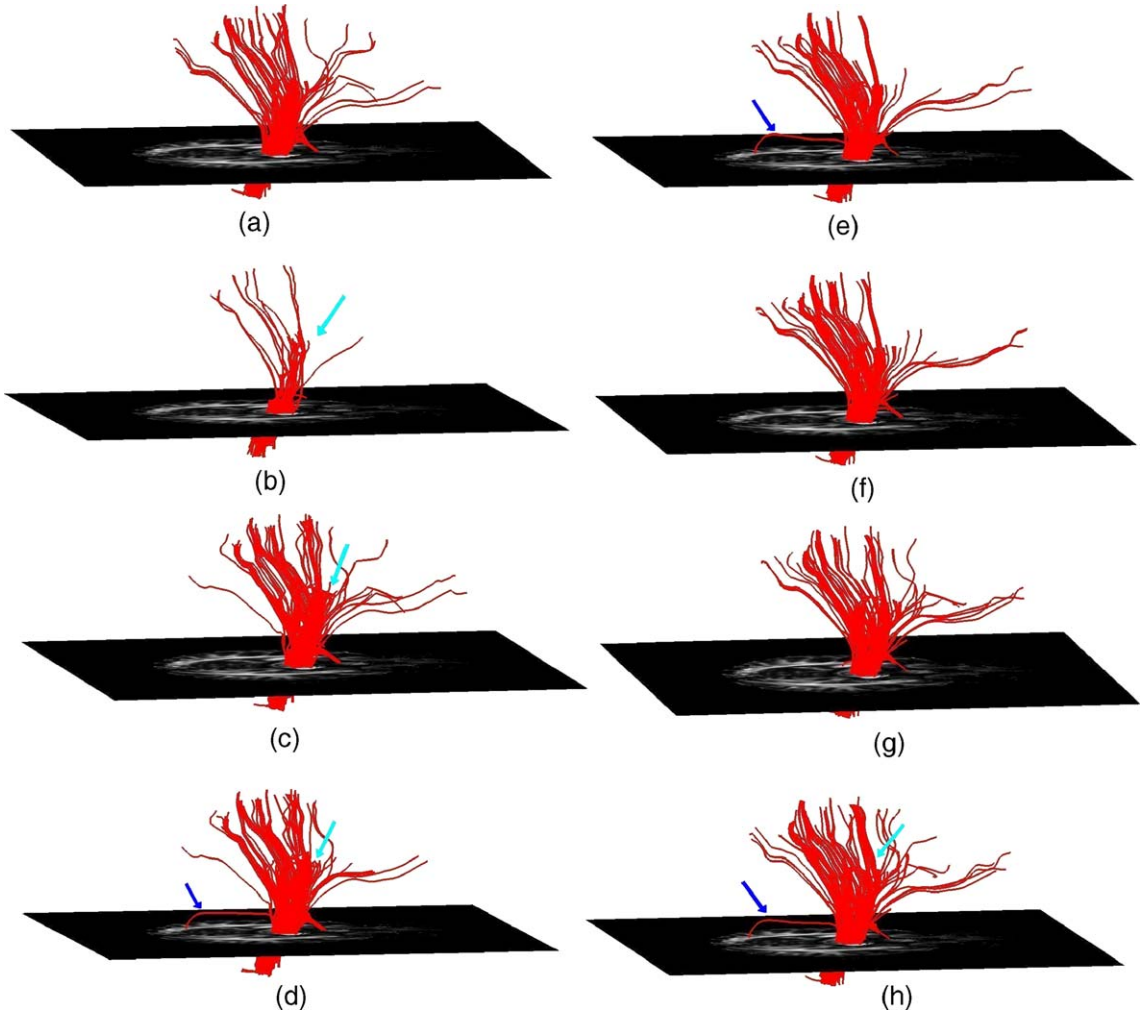

Fig. 9. Oblique view of an axial slice with reconstructed fibers seeded in the projection pathways. Panels a–d are from linear, nearest neighbor, cubic polynomial and spline interpolations respectively, and panels e–h are from the anisotropic interpolation with a_{max} = 5, 10, 15 and 20 respectively. Arrow in panel b points to missing fibers, and cyan arrows in panels c, d, h point to possibly erroneous dense fibers. Blue arrows in panels d, e, h indicate another erroneous fiber pathway at the base.

In summary, this study has established a unified framework for anisotropic interpolation and smoothing of DTI data. The integrated scheme provides a smooth, continuous and boundary preserved tensor field for reconstruction of fiber tracts. A smooth and continuous tensor field allows quantification of high order geometrical properties, such as curvature and torsion, of reconstructed fiber tracts, and the boundary preservation capability improves the accuracy of fiber tracking by confining fiber tracts within the anatomical structure of interest. In addition, the new interpolation has compact support, reasonably low computational complexity, and more flexible frequency response than conventional interpolation methods. Enhanced performance in fiber tracking with both synthetic and in vivo DTI data has proven the effectiveness of this unified interpolation and smoothing framework.

Acknowledgments

The authors are very grateful to Professor Benoit Dawant (Department of Electrical Engineering and Computer Science, Vanderbilt University) for generously providing the 3D visualization tool. Thanks are also given to Professor Akram Aldroubi (Department of Mathematics) for his valuable comments and discussions. This work was supported by NIH grants R01EB000461 funded to John C. Gore and R01EB02777 funded to Adam W. Anderson.

References

Anderson, A.W., 2001. Theoretical analysis of the effects of noise on diffusion tensor imaging. Magn. Reson. Med. 46, 1174–1188.

Basser, P.J., Mattiello, J., LeBihan, D., 1994. MR diffusion tensor spectroscopy and imaging. Biophys. J. 66, 259–267.

Basser, P.J., Pajevic, S., Pierpaoli, C., Duda, J., Aldroubi, A., 2000. In vivo fiber tractography using DT-MRI data. Magn. Reson. Med. 44 (4), 625–632.

Chen, B., Hsu, E.W., 2005. Noise removal in magnetic resonance diffusion tensor imaging. Magn. Reson. Med. 54 (2), 393–401.

Conturo, T.E., Lori, N.F., Cull, T.S., Akbudak, E., Snyder, A.Z., Shimony, J.S., McKinstry, R.C., Burton, H., Raichle, M.E., 1999. Tracking neuronal fiber pathways in the living human brain. Proc. Natl. Acad. Sci. U. S. A. 96 (18), 10422–10427.

Coulon, O., Alexander, D.C., Arridge, S., 2004. Diffusion tensor magnetic resonance image regularization. Med. Image Anal. 8 (1), 47–67.

Ding, Z., Gore, J.C., Anderson, A.W., 2003. Classification and quantification of neuronal fiber pathways using diffusion tensor MRI. Magn. Reson. Med. 49 (4), 716–721.

Ding, Z., Gore, J.C., Anderson, A.W., 2005. Reduction of noise in diffusion tensor images using anisotropic smoothing. Magn. Reson. Med. 53 (2), 485–490.

Gossl, C., Fahrmeir, L., Putz, B., Auer, L.M., Auer, D.P., 2002. Fiber tracking from DTI using linear state space models: detectability of the pyramidal tract. NeuroImage 16, 378–388.

Jones, D.K., Simmons, A., Williams, S.C., Horsfield, M.A., 1999. Non-invasive assessment of axonal fiber connectivity in the human brain via diffusion tensor MRI. Magn. Reson. Med. 42 (1), 37–41.

Lazar, M., Weinstein, D.M., Tsuruda, J.S., Hasan, K.M., Arfanakis, K., Meyerand, M.E., Badie, B., Rowley, H.A., Haughton, V., Field, A., Alexander, A.L., 2003. White matter tractography using diffusion tensor deflection. Hum. Brain Mapp. 18 (4), 306–321.

Le Bihan, D., Mangin, J.F., Poupon, C., Clark, C.A., Pappata, S., Molko, N., Chabriat, H., 2001. Diffusion tensor imaging: concepts and applications. J. Magn. Reson. Imaging 13, 534–546.

Lehmann, T.M., Gonner, C., Spitzer, K., 1999. Survey: interpolation methods in medical image processing. IEEE Trans. Med. Imag. 18, 1049–1075.

Lu, Y., Aldroubi, A., Gore, J.C., Anderson, A., Ding, Z., in press. Improved diffusion tensor tractography using Bayesian fiber tracking. NeuroImage.

Mori, S., van Zijl, P.C., 2002. Fiber tracking: principles and strategies—A technical review. NMR Biomed. 15 (7–8), 468–480.

Mori, S., Crain, B.J., Chacko, V.P., van Zijl, P.C., 1999. Three-dimensional tracking of axonal projections in the brain by magnetic resonance imaging. Ann. Neurol. 45, 265–269.

Pajevic, S., Aldroubi, A., Basser, P.J., 2002. A continuous tensor field approximation of discrete DT-MRI data for extracting microstructural and architectural features of tissue. J. Magn. Reson. 154, 85–100.

Parker, G.J., Schnabel, J.A., Symms, M.R., Werring, D.J., Barker, G.J., 2000. Nonlinear smoothing for reduction of systematic and random errors in diffusion tensor imaging. J. Magn. Reson. Imag. 11, 702–710.

Poupon, C., Clark, C.A., Frouin, V., Regis, J., Bloch, I., LeBihan, D., Mangin, J.F., 2000. Regularization of diffusion-based direction maps for the tracking of brain white matter fascicles. NeuroImage 12, 184–195.

Tench, C.R., Morgan, P.S., Blumhardt, L.D., Constantinescu, C., 2002. Improved white matter fiber tracking using stochastic labeling. Magn. Reson. Med. 48, 677–683.

Tournier, J.D., Calamante, F., King, M.D., Gadian, D.G., Connelly, A., 2002. Limitations and requirements of diffusion tensor fiber tracking: an assessment using simulations. Magn. Reson. Med. 47 (4), 701–708.

Wang, Z., Vemuri, B.C., Chen, Y., Mareci, T., 2003. A constrained variational principle for direct estimation and smoothing of the diffusion tensor field from DWI. In: Taylor, C.J., Noble, J.A. (Eds.), Information Processing in Medical Imaging. Springer-Verlag, Heidelberg, pp. 660–671.

Weickert, J., 1999. Coherence-enhancing diffusion filtering. Int. J. Comput. Vis. 31, 111–127.

Westin, C.F., Maier, S.E., Mamata, H., Nabavi, A., Jolesz, F.A., Kikinis, R., 2002. Processing and visualization for diffusion tensor MRI. Med. Image Anal. 6 (2), 93–108.

Xu, D., Mori, S., Solaiyappan, M., van Zijl, P.C., Davatzikos, C., 2002. A framework for callosal fiber distribution analysis. NeuroImage 17, 1131–1143.

Xue, R., van Zijl, P.C.M., Crain, B.J., Solaiyappan, M., Mori, S., 1999. In vivo three-dimensional reconstruction of rat brain axonal projections by diffusion tensor imaging. Magn. Reson. Med. 42, 1123–1127.